Journal of Materials Chemistry A

PAPER

View Article Online
View Journal | View Issue

Cite this: J. Mater. Chem. A, 2016, 4, 9850

Nanostructured polymeric yolk–shell capsules: a versatile tool for hierarchical nanocatalyst design†

Noelia M. Sanchez-Ballester,‡[ab] Gaulthier Rydzek,‡*[ac] Amir Pakdel,[a] Anjaneyulu Oruganti,[d] Kotone Hasegawa,[a] Masanori Mitome,[a] Dmitri Golberg,[a] Jonathan P. Hill,[a] Hideki Abe[d] and Katsuhiko Ariga*[a]

Received 21st April 2016
Accepted 23rd May 2016

DOI: 10.1039/c6ta03311c

www.rsc.org/MaterialsA

The concept of all-polymeric yolk–shell nanocapsules as a tunable platform for designing hierarchically nanostructured catalysts is demonstrated. Such nanocapsules are investigated for catalytic CO oxidation. Polyaniline yolk–shell nanocapsules are synthesized in one pot, without a template and characterized by UV-Visible, IR, XRD, DLS, BET, TEM and EDS analyses. The yolk and shell parts of nanocapsules can be selectively doped: yolk-trapping of copper ions allows the *in situ* synthesis of yolk-confined copper NPs. Hierarchical co-loading with gold (shell) and copper (yolk) can also be performed. By investigating the catalytic activities of all possible architectures with Cu and Au, the benefits of controlling the catalyst nanostructure and its hierarchical loading are demonstrated. Both confinement and cooperative effects are measured with a respective increase of catalysis performances of 2 and 7 times. Nickel can be loaded in the yolk part instead of copper, and platinum (shell) instead of gold, demonstrating that this catalyst design strategy is adaptable. A similar trend for catalysis performances is obtained with nickel based catalysts. Due to its polymeric nature, this yolk–shell platform is anticipated to be able to trap a large variety of catalytic centers, allowing the on-demand design of catalysts. Applications for gas catalysis, electrocatalysis, fuel cells, and water splitting are anticipated.

Introduction

Because of current environmental sustainability challenges, it is imperative that society collectively addresses the deleterious aspects of emission control,[1] pharmaceutical synthesis[2] and energy production.[3,4] A potential solution to these issues lies in the use of nanostructured catalysts obtained, for instance, by the immobilization of appropriate materials on nanostructured mesoporous supports.[4,5] The properties of thus-formed materials are in many cases influenced by the surface structure.[6,7] More specifically, interface-confined catalysts have been found to exhibit confinement effects[8–10] while the formulation of hollow core–shell nanocatalysts has become an active research field.[11–14] The attractive features of these systems might be developed to a higher level by the hierarchical integration of several catalytic centers in a nanostructured matrix.[15,16] The aim of the present study is to demonstrate the potential of self-assembled nanostructured polymeric materials in the design and synthesis of tunable hierarchical nanocatalysts. An ideal nanostructured matrix for designing catalysts should possess the following properties: (i) a well-defined yolk–shell structure for the effective containment and protection of catalytic centers, which also introduces the possibility of confinement effects, (ii) versatile physical and chemical properties allowing the immobilization of different catalytic centers in a hierarchical manner, and (iii) good transport properties within the nanostructures promoting cooperative effects between the catalytic centers. Here, we introduce the general synthesis concept of a tunable hierarchical nano-structured catalyst, based on polyaniline (PANI), and that exhibits the properties described in (i)–(iii). PANI is one of the most promising conducting polymers due to its simple and inexpensive synthesis[17] and because the resulting polymer chains tend to self-organize into a variety of supramolecular structures including hollow spheres and all-polymer yolk–shell nanocapsules.[18,19] In addition, PANI's stability at high temperature, chemical versatility, and intrinsic porosity make it a good candidate for designing nanostructured catalysts.[20–22]

[a]World Premier International (WPI) Research Center for Materials Nanoarchitectonics (MANA), National Institute for Materials Science (NIMS), 1-1 Namiki, Tsukuba 305-0044, Japan. E-mail: RYDZEK.Gaulthier@nims.go.jp; ARIGA.Katsuhiko@nims.go.jp

[b]Institut Charles Sadron, Centre National de la Recherche Scientifique, Université de Strasbourg, 23 rue du Loess, 67034 Strasbourg Cedex 2, France

[c]International Center for Young Scientists (ICYS), Tsukuba, Ibaraki 3050047, Japan

[d]Catalytic Materials Group, Environmental Remediation Materials Unit, Environment and Energy Materials Division, National Institute for Materials Science (NIMS), 1-1 Namiki, Tsukuba 305-0044, Japan

† Electronic supplementary information (ESI) available: Characterization, controls, and data. See DOI: 10.1039/c6ta03311c

‡ These authors contributed equally.

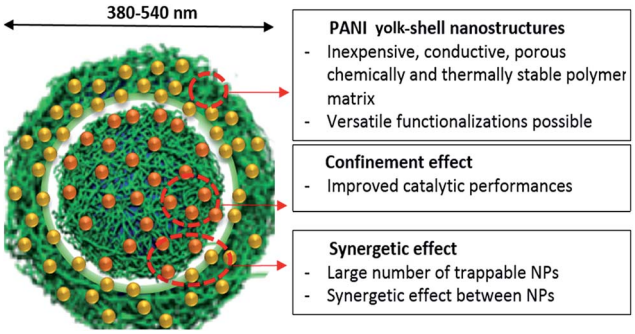

Fig. 1 Schematic depiction of hierarchically NP-loaded PANI yolk–shell nanocapsules and their anticipated properties. The PANI matrix is anticipated to provide an exceptional platform for catalysis thanks to its nanostructured reactor form, intrinsic porosity, and its selective doping abilities. Depending on the targeted reaction, the choice of entrapped metallic nanoparticles plays a key role, as well as PANI's intrinsic properties. As a proof of concept, in order to enhance CO oxidation, Cu NPs were grown in the yolk part and Au NPs in the shell.

Here, all-polymer template-free PANI yolk–shell nanocapsules were used as a matrix for the hierarchical integration of metallic cations by achieving a confined doping of Cu, Ni and Au ions. Subsequent *in situ* growth of metallic NPs could be achieved by chemical reduction (Fig. 1). PANI yolk–shell nanocapsules, hierarchically loaded with multiple types of NP, were tested for catalytic carbon monoxide (CO) oxidation at 150 and 300 °C.

Experimental

Materials

Copper sulfate pentahydrate ($CuSO_4 \cdot 5H_2O$, $M = 249.7$ g mol^{-1}, CAS 7758-99-8), gold chloride ($HAuCl_4 \cdot 4H_2O$, $M = 411.9$ g mol^{-1}, CAS 2798-77-8), copper nanopowder (60 nm, CAS 7440-50-8), nickel nanopowder (CAS 7440-02-0), ethylenediaminetetraacetic acid (EDTA, $M = 292.24$ g mol^{-1}, CAS 60-00-4), and platinum chloride ($PtCl_2$, $M = 265.99$ g mol^{-1}, CAS 10025-65-7) were purchased from Sigma Aldrich. Hydrazine (N_2H_4, $M = 50.06$ g mol^{-1}, CAS 688-00906), nickel nitrate ($Ni(NO_3)_2 \cdot 6H_2O$, $M = 290.79$ g mol^{-1}, CAS 24302-52), potassium peroxydisulfate (KPS, $K_2S_2O_8$ $M = 270.32$ g mol^{-1}, CAS 169-11891), and aniline (ANI, $M = 93.1$ g mol^{-1}, CAS 62-53-3) were purchased from Wako and used as received.

Synthesis of PANI yolk–shell nanocapsules

All solutions were prepared using absolute ethanol (VWR, 99.5% purity) and MilliQ water (18.2 MΩ cm^{-1}) purified using a Purelab Prima system. Reaction mixtures were composed of 10 mM $CuSO_4$, 20 mM aniline and 40 mM KPS. Aniline (2 mmol) was first dissolved in cold ethanol (5 mL) in a round-bottomed flask cooled in an ice bath. Cold water (35 mL) and aqueous 0.2 M $CuSO_4$ solution (5 mL) were added. The obtained solution turned greenish blue upon complexation of aniline with Cu(II) ions. After 10 minutes, polymerization was commenced by the addition of a pre-cooled saturated KPS solution (55 mL). The solution color turned brown after a few minutes while colloids were being polymerized. The reaction was allowed to proceed overnight (12 h), leading to a black dispersion of colloids. At this stage, the dispersion was mainly composed of PANI nanospheres and reaction byproducts.

Purification of capsules. The colloidal dispersion was centrifuged at 4500 rpm for 10 min, washed and sonicated for 2 minutes by using water (3 times) and then acetone (2 times). After these 5 washing cycles, a last cycle was performed with water. At this stage, the colloidal dispersion was composed of yolk–shell nanocapsules doped with copper ions (originating from the synthesis step). After freeze drying overnight (12 h), a black powder was obtained.

Removal of initial copper ions. For the sake of reproducibility and comparison between the different systems, this treatment was applied to every sample, even when PANI was subsequently re-doped with copper ions. "Empty" nanocapsules were obtained by treating the "as prepared" nanocapsules (110 mg) twice with an aqueous EDTA solution (10 g L^{-1}) under stirring for 24 h. The resulting nanocapsules were washed with a 0.1 M NaOH solution, sonicated for 2 minutes and centrifuged 3 times at 4500 rpm for 10 min. At this stage, copper-free nanocapsules were obtained, with adsorbed EDTA molecules. After freeze drying overnight (12 h), a black powder was obtained.

Ionic loading. Ionic loading was always performed on dedoped PANI capsules (after 48 h treatment with EDTA). Ionic loading was performed by dispersing 60 mg of the resulting nanocapsules into a 0.2 M solution of either $CuSO_4$ or $NiCl_2$ for 24 h. After 3 washing cycles with water (sonication for 2 minutes, centrifugation for 10 minutes at 4500 rpm), the fully copper-loaded capsules were freeze dried overnight (12 h).

Kinetic ionic confinement. To obtain yolk-loaded nanocapsules, EDTA treatment (10 g L^{-1}) was applied to fully (Ni or Cu) loaded capsules for 2 h. The resulting dispersion was purified by two washing cycles with water (sonicated for 2 minutes and centrifuged at 4500 rpm for 10 min), then one washing cycle with acetone and finally one more washing cycle with water. After freeze drying overnight (12 h), a black powder was obtained.

***In situ* NP reduction.** The nanocapsules (50 mg) were dispersed in water (20 mL) and heated at 80 °C in the presence of hydrazine (20 mL) for 3 h. The resulting materials underwent 2 washing cycles with water (sonicated for 2 minutes and centrifuged at 4500 rpm for 10 min), one with acetone and one more with water. The resulting nanocapsules were freeze dried overnight (12 h). As a precaution to avoid any oxidation of metallic copper (nickel), the nanocapsule powders were stored under vacuum.

Shell functionalization with Au or Pt NPs. The nanocapsules (50 mg) were stirred for 3 h in a gold seeding solution containing $HAuCl_4$ (0.05%) and NaOH (10^{-2} M). The resulting dispersion was centrifuged at 4500 rpm for 10 min and then redispersed in a fresh solution (10 mL) containing 1 M K_2CO_3 and 0.5% $HAuCl_4$. After 10 min, formaldehyde (37% w/v soln (aq.), 5 mL) was added and the reduction reaction was allowed to proceed for 30 minutes under gentle stirring. The final product

underwent 2 washing cycles with water (sonicated for 2 minutes and centrifuged at 4500 rpm for 10 min), one with acetone and one more with water. A Pt shell was obtained by dispersing the nanocapsules in a freshly prepared solution containing 1 M K_2CO_3 and 0.5% $PtCl_2$ (10 mL) and then adding formaldehyde (37% w/v soln (aq.), 10 mL) with a subsequent reaction for 1 h. All the obtained nanocapsule powders were stored under vacuum.

Catalytic activity measurements

The CO oxidation reaction was implemented using a circulating-gas reactor equipped with a gas chromatograph (Shimadzu GC-8A). Nanocapsule-based catalysts were vacuum-dried in the reactor for 1 h at 150 °C prior to catalysis. During the measurement, a mixture of CO (6.67 kPa) and O_2 (3.33 kPa) was circulated through the catalyst at 150 °C and 300 °C. Oxidation of CO to CO_2 was monitored by using gas chromatography. Conversion rate results were normalized with respect to their copper or nickel contents obtained from ICP analysis.

Characterization

Scanning transmission electron microscopy (STEM) was performed using a Hitachi S-4800 at an accelerating voltage of 30 kV. The samples were observed directly on copper grids after 15 min of drying under vacuum. Transmission electron microscopy (TEM), energy-dispersive X-ray spectroscopy (EDS) and high-angle annular dark field-scanning transmission electron microscopy (HAADF-STEM) were performed by using a JEM-2100 (JEOL) transmission electron microscope (accelerating voltage, 200 kV) equipped with a CCD camera. Molybdenum grids were used during EDS analysis. Au NP distribution analysis was performed on 3 different TEM micrographs by using the ImageJ software. UV-Visible spectroscopy was performed using a Shimadzu (Japan) UV visible NIR spectrophotometer (model UV-3600). Attenuated total reflection infrared spectroscopy (ATR-FTIR) on PANI nanocapsule powders was performed using a Thermoscientifique Nicolet 4700 apparatus (USA). Powder X-ray diffractometry (pXRD) was performed using a Panalytical X'pert with CuK_α radiation ($\lambda = 1.5418$ Å) in the range from 5 to 100 degrees. Dynamic light scattering (DLS) and flow-cell zeta-potential measurements were performed on PANI nanocapsules dispersed in water at 25 °C by using a Beckman Coulter apparatus. DLS results were obtained by accumulating 70 measurement times. Zeta potential was obtained by accumulating 10 measurement times and sampling during 400 μs with an applied electric field of -16.38 V cm^{-1}. Brunauer–Emmett–Teller measurements (BET) and N_2 adsorption–desorption isotherms were recorded using an automatic adsorption instrument (Quantachrome Instrument, Autosorb-1 U.S.A.) in order to determine the surface areas of the samples. For each measurement, about 30 mg of the sample was taken and degassed for 24 h at 100 °C prior to the measurement. The adsorption–desorption isotherms were recorded at a liquid nitrogen temperature of 77.35 K. The specific surface area was calculated using the Brunauer–Emmett–Teller (BET) method in a relative pressure range (P/P_0) of 0.05–0.30. Inductively coupled plasma optical emission spectrometry (ICP-OES) was performed on a 20 mg sample of each type of nanocapsules by using an ICPS8100CL model spectrometer. Thermal gravimetry analysis (TGA) was performed on 15 mg capsules by using a Hitachi HT-Seiko Instrument Exter 6300 X-ray Photoelectron Spectroscopy. XPS was carried out on an ESCALAB Mark II (VG Company, U.K.). Energies were calibrated as C 1s at 285 eV.

Results and discussion

Synthesis and characteristics of PANI yolk–shell nanocapsules

Template-free synthesis of nanostructured catalysts is a fast growing research field, owing to their promising "nanoreactor" form.[23–25] From this point of view, semi-rigid rod-like polymeric materials like PANI present the advantage that they undergo spontaneous self-organization processes under mild conditions in water and offer a variety of post-assembly modifications.[5,26] In this study, Cu(II) ions were used both as a catalyst for aniline polymerization and as a structuring agent for the formation of PANI template-free yolk–shell nanocapsules in the presence of potassium persulfate (KPS).[19,27] On mixing aniline with $CuSO_4$, the emergence of an absorption peak at 370 nm measured by UV-Visible spectroscopy suggested complexation and partial oxidation of aniline by Cu(II) ions (Fig. S-1a†). After 12 h oxidation by using KPS, a PANI salt dispersion was obtained whose UV-spectrum contains 3 absorption bands at 330, 480 and 750 nm, corresponding to the emeraldine salt form.[28] Under alkaline conditions, a typical emeraldine base spectrum was also obtained, with benzenoid segments absorbing around 350 nm and quinonoids around 700 nm (Fig. S-1b and c†).[29,30] Although it is well known that PANI can present crystalline domains, powder X-ray diffraction (pXRD) analysis of PANI nanocapsules revealed an amorphous structure leading to broad and low intensity peaks around 15°, and 20° suggesting a poor parallel periodicity of PANI chains (Fig. S-2†).[31] The observation of PANI dispersion by using scanning transmission electron microscopy (STEM) revealed nanostructured yolk–shell capsules with diameters between 380 and 500 nm, containing a 200 nm "yolk" and a shell of thickness 40 nm (Fig. 2a to e). This result is consistent with DLS measurements in water where

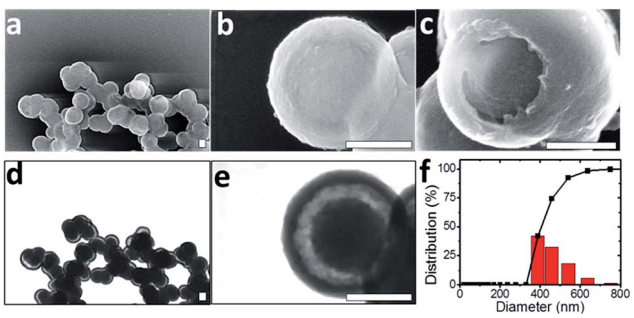

Fig. 2 General characterization of PANI yolk–shell nanocapsules. STEM micrographs of PANI yolk–shell nanocapsules obtained in scanning (a–c) and transmission (d and e) modes. All scale bars represent 200 nm. Corresponding cumulative and relative size distributions measured by DLS in water (f).

an average particle size of 459 nm was found with a narrow diameter distribution, with 93% of capsules falling in the range of 380 to 540 nm (Fig. 2f). This result also demonstrates that PANI nanocapsules are efficiently dispersed and non-aggregated in solution after sonication.

Interestingly, only PANI nanospheres were observed by STEM of the raw synthetic products, while the yolk–shell structure was observed on purified samples (Fig. S-1d and e†). Washing procedures appear to remove the more soluble PANI chains (shorter or less doped) from the interiors of PANI spheres as has recently been described by Sun *et al.*[32] At higher magnifications, the TEM micrographs of yolk–shell nanostructures revealed no crystallinity, in agreement with pXRD data (Fig. S-2b and c†). These PANI nanocapsules are easily redispersible in water, probably due to a slightly positive surface charge (+2.54 mV), and exhibited a specific surface area of 55 ($\pm$5) $m^2\ g^{-1}$ with a mesopore size distribution centered at 3.8 nm diameter (Fig. S-2d and e†), in accordance with recent studies demonstrating the superior sorption abilities of PANI structures.[19,20] The forms of these yolk–shell nanocapsules are mainly preserved over a wide pH range from 1 to 14. They are also stable after treatment with EDTA. These features indicate a promising future for PANI yolk–shell nanocapsules as building blocks of materials in aqueous solutions (Fig. S-3†). The PANI structures could also undergo drying, heating at 300 °C and vacuum processes, rendering these capsules suitable for gas phase catalysis (Fig. S-3†). Cross-linking PANI capsules with formaldehyde seemed to further increase their thermal stability (Fig. S-2f†).

Selective doping of nanocapsules

PANI is a semi-rigid linear conjugated polymer composed of benzenoid and quinonoid units whose physical properties can be tuned by acid or ion doping.[33] It is anticipated that the combination of doping properties with the present specific yolk–shell nanostructure will allow the design and synthesis of a wide variety of hierarchically-structured catalysts. EDS elemental analysis of the as-prepared nanocapsules revealed the doping of PANI with sulfate and copper ions from $CuSO_4$ during polymerization (Fig. S-4†). Copper ions are indeed known to interact with benzenoid and quinonoid segments, leading to partial oxidation of PANI.[34] This process was confirmed by using ATR-FTIR spectroscopy and with the monitoring of the $\nu_{N=Q=N}$ characteristic quinonoid band described by MacDiarmid.[35] $CuSO_4$-doped PANI nanocapsules exhibited a broad band at 1148 cm^{-1} with a shoulder at 1170 cm^{-1} (Fig. S-5†).[36]

Upon dedoping by using an EDTA salt or by reducing copper ions with hydrazine,[37] the peak at 1148 cm^{-1} disappeared while the absorption at 1170 cm^{-1} increased (Fig. 3). The ratio between these peaks changed from around 1.4 for the copper ion doped state to 0.6 for the undoped state (Fig. 3b). When $CuSO_4$-doped PANI nanocapsules were treated with a 2.7×10^{-2} M EDTA solution, the cations trapped in the shell layer were removed after 2 h (Fig. S-6†). These results suggest that EDTA can diffuse through the mesoporous PANI matrix, complex the copper ions present there and remove them by subsequent

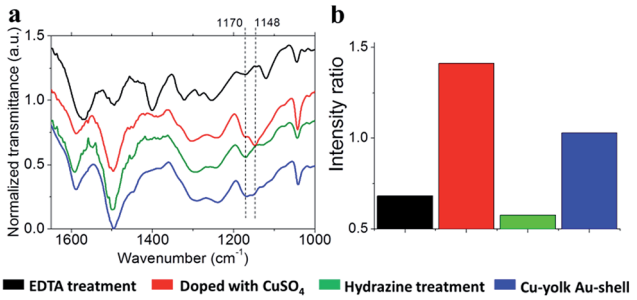

Fig. 3 Doping and dedoping of PANI. (a) Typical ATR-FTIR spectrum of PANI yolk–shell nanocapsules after loading with Cu(II) (red line), after treatment with EDTA for 48 h (black line), after localized copper reduction in the yolk using hydrazine (green line) and after gold shell deposition (blue line). Peaks at 1170 and 1148 cm^{-1}, characteristic of doped and undoped states with copper ions, are labelled. (b) Evolution of the normalized absorbance ratio between peaks at 1148 cm^{-1} (doped state) and 1170 cm^{-1} (undoped state). Ratios were calculated from zoomed baseline corrected plots of 1170 and 1148 cm^{-1} peaks (Fig. S-5†).

washing. However, ionic and hydrogen bonding interactions also allowed the trapping of EDTA within PANI nanocapsules, leading to a surface charge reversal at −29 mV (Fig. S-7†). This phenomenon is well known when multiple charged molecules are used to functionalize surfaces, for instance, by using a layer-by-layer approach.[38] Upon adsorption of EDTA, an electrostatic potential barrier is induced which opposes the diffusion of more EDTA molecules within the PANI matrix. As a result, a treatment time of 48 h was required for the removal of the cations contained in the yolk regions of the capsules (Fig. S-6†). This shielding effect, combined with the yolk–shell nanostructure, facilitates the selective doping of PANI leading to confinement of cations in the yolk part, as described in Fig. S-8.†

In situ growth of metallic NP

Chemical or electrochemical *in situ* reduction of complexed copper ions in a PANI matrix has been demonstrated to generate dispersed NPs.[39,40] Here, the growth of Cu NPs was achieved by the chemical reduction of yolk-confined copper ions. These ions necessitated strong reducing conditions to be converted into metallic copper, probably because they are buried into a mesoporous electroactive PANI matrix. For instance, reduction by formaldehyde did not work. Reduction by hydrazine treatment at 80 °C was performed, and the resulting capsules were investigated by TEM, UV-Vis and IR spectroscopies and pXRD. As a small, non-charged molecule, hydrazine diffuses through PANI matrices, experiencing any shielding effects and can react with any confined doping ions. Reduction of copper ions within the PANI matrix can be seen as a dedoping process, and was monitored by observing the elimination of the 1148 cm^{-1} band from its IR spectrum (Fig. 3).[35] After a 3 h treatment, the PANI spectrum exhibited a dedoped structure similar to the one obtained following EDTA treatment (Fig. 3b). TEM-EDS analysis of the resulting material revealed that copper was still confined in the yolk part of

nanocapsules following reduction with accompanying emergence of an electron diffraction pattern (Fig. 4 and S-9†). The presence of crystalline materials in reduced Cu-yolk nanocapsules was confirmed by pXRD analysis where a low intensity peak at 43.23° assigned to the (111) reflection of metallic copper (JCPDS 5-0661) was observed (Fig. S-10†). The low intensity of the pXRD peaks could be due to the poor crystallinity of the sample but also due to the presence of only a small proportion of Cu NPs contained within an amorphous PANI matrix. Hydrazine treatment was also found to reduce PANI as observed by UV-Vis spectroscopy where a red shift of the benzenoid absorption band and a decrease of the quinonoid band intensity occurred (Fig. S-11†). In the subsequent step, gold was chosen for the decoration of the shell part of yolk–shell nanocapsules, since Au NPs are of broad interest for several applications ranging from catalysis to optical and biological fields.

Shell functionalization

Au-shell deposition was achieved by following a "seeding" strategy, leading to both the reoxidation of PANI benzenoid segments (Fig. S-11†) and the surface decoration of nanocapsules with gold NPs. The analysis of TEM images allowed to determine that most gold NPs ranged from 1 to 15 nm, with 90% of them being smaller than 30 nm in diameter (Fig. 4c and 5). Consistent with the literature, the reduction of gold ions was largely spontaneous, owing to PANI and Au(III) standard reduction potentials, and as testified by the oxidation of benzenoid segments (Fig. S-11†).[41] As a consequence, only the outer shell of the capsules was functionalized and no gold could be detected inside the capsules (Fig. 4c). The design of hierarchically loaded nanocapsules was thus advantageously eased when depositing noble

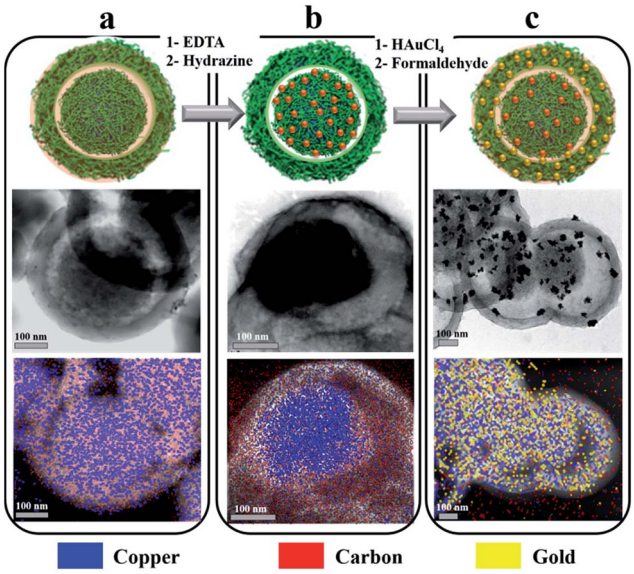

Fig. 4 Reduction of yolk-confined copper ions and gold shell deposition. Schematic representations and TEM-EDS micrographic analyses of PANI yolk–shell nanocapsules fully doped with copper ions (a), after the reduction of yolk-confined Cu ions with hydrazine (b), or after achieving the (Cu-yolk Au-shell) hierarchical architecture (c).

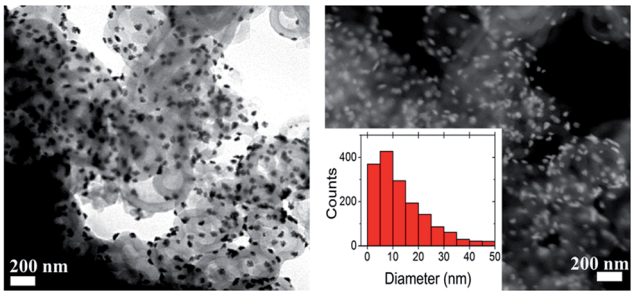

Fig. 5 Cu-yolk Au-shell architecture. Typical TEM micrographs, in dark field and bright field modes, of (Cu yolk Au shell) hierarchically loaded nanocapsules. The Au-NP size distribution, calculated from 3 TEM micrographs, is in the inset.

metals on the shell part. However, when a 10% formaldehyde solution was used as a reductant for gold, a more uniform surface decoration with smaller gold NPs was obtained, more suitable for catalysis (Fig. S-12†). During the functionalization of the shell with gold NPs, a partial dissolution of metallic copper in the yolk was observed, generating locally Cu(II) ions and leading to ionic redoping of the PANI shell region as indicated by EDS and ATR-FTIR (Fig. 3 and 4c). However, pXRD analysis revealed the presence of both metallic gold and copper, with peaks at 37.81 and 43.95° respectively attributed to the (111) and (200) reflections of metallic gold (JCPDS 4-0783) and peaks at 43.23° and 50.48° respectively attributed to the (111) and (200) reflections of metallic copper. No other impurities or alloys could be detected (Fig. S-10†). The PANI shell, previously reduced during the hydrazine treatment to achieve the Cu-yolk architecture, could thus successfully reduce gold ions and refrain total dissolution of metallic copper in the yolk part. XPS analysis of Cu 2p in PANI nanocapsules either doped with Cu(II) or after achieving the (Cu-yolk Au-shell) architecture allowed to confirm this mechanism (Fig. S-13†). Cu(II)-doped PANI nanocapsules exhibited 2 peaks at 934.9 eV (Cu $2p_{3/2}$) and 955.2 eV (Cu $2p_{1/2}$) as well as satellite peaks indicating the presence of Cu(II) ions. By decomposition of the Cu $2p_{3/2}$ peak, both Cu(II) and Cu(I) oxidation states were found in Cu(II)-doped nanocapsules at 935 eV and 932.4 eV, respectively, confirming the ability of Cu(II) to partially oxidize PANI.[42,43] In the case of the (Cu yolk Au shell) architecture, satellite peaks were largely attenuated and decomposition of the Cu $2p_{3/2}$ peak identified Cu(II) and Cu(0) oxidation states at 934.3 eV and 932.6 eV, respectively.[42,44] The simultaneous presence of Au(0) was testified by the Au $4f_{5/2}$ and Au $4f_{7/2}$ peaks at 84 and 87.6 eV, respectively (Fig. S-14†). By both protecting the yolk-confined copper from total oxidation and inducing the gold reduction on the shell part, PANI eases the design of hierarchically loaded nanostructures, demonstrating the advantage of an electroactive yolk–shell polymeric structure for assembling multimetallic catalysts.

Catalytic activity

As a proof of concept, the catalytic activity of hierarchically loaded yolk–shell nanocapsules was investigated for CO oxidation. Both gold and copper are known for efficiently catalyzing

the oxidation of many components in ambient air at low temperatures,[45] particularly CO.[46–48] However recent studies demonstrated that the dispersion of active centers on a reducible support able to trap and provide oxygen during the reaction, for instance CeO_2, is crucial for achieving high catalysis performances.[49,50] PANI cumulates both the electroactivity and the ability to trap and activate O_2 molecules through its Lewis acid centers (doped nitrogen atoms, trapped cations),[51–53] while it can also chemisorb CO molecules on its Lewis base centers (undoped nitrogen atoms).[54,55] It is thus expected to be a suitable support matrix for CO oxidation with gold and copper. Moreover, TGA and STEM investigations of the as-prepared and (Cu yolk Au shell) nanocapsules at 300 degrees exhibited good thermal stability with no significant structural change contrary to the capsules heated up to 450 degrees (Fig. S-2 and S-15†). A systematic investigation was conducted at each functionalization step of PANI yolk–shell nanocapsules in order to detect any eventual confinement or cooperative effects for embedded Cu and Au NPs (Fig. S-16†). The activities of PANI nanocapsules loaded with copper ions, Cu yolk, Cu yolk–shell and (Cu-yolk Au-shell), were thus measured (Fig. 6) and normalized by their copper contents (obtained by ICP analysis, Table S-1†). A commercial copper nanopowder (60 nm) was used as the control (blue line on Fig. 6).

To establish the proof of concept of hierarchically loaded nanocatalysts, this work focused on three points: the identification of the catalytic centers in the system (i), significance of the catalyst nanostructure (ii) and significance of the hierarchical architecture. In this regard, commercial copper NP, copper ion loaded nanocapsules, Cu-yolk–shell and Au-shell nanocapsules were used as controls while Cu-yolk and (Cu-yolk Au-shell) nanocapsules were the targeted catalysts.

Identification of the main catalytic centers. Since copper ions as well as amine-containing polymers may exhibit some catalytic properties, the activity of copper ion loaded nanocapsules was tested, resulting in a low CO_2 conversion rate at both 300 °C and 150 °C (dotted line in Fig. 6). As a comparison, commercial copper NPs were at least two times more efficient, reaching up to 13% conversion rate at 300 °C. As expected, this result confirms that metallic centers like copper or gold NPs will be the main catalytic centers for CO activation in functionalized PANI yolk–shell nanocapsules.

Significance of the catalyst nanostructure. By comparing the catalysis performances of Cu-yolk nanocapsules (where metallic copper is confined in the yolk part, green line in Fig. 6), with Cu-yolk–shell nanocapsules (with no nanostructures, grey line) and commercial copper NPs (blue line), the influence of the catalyst nanostructure was investigated. Non-structured

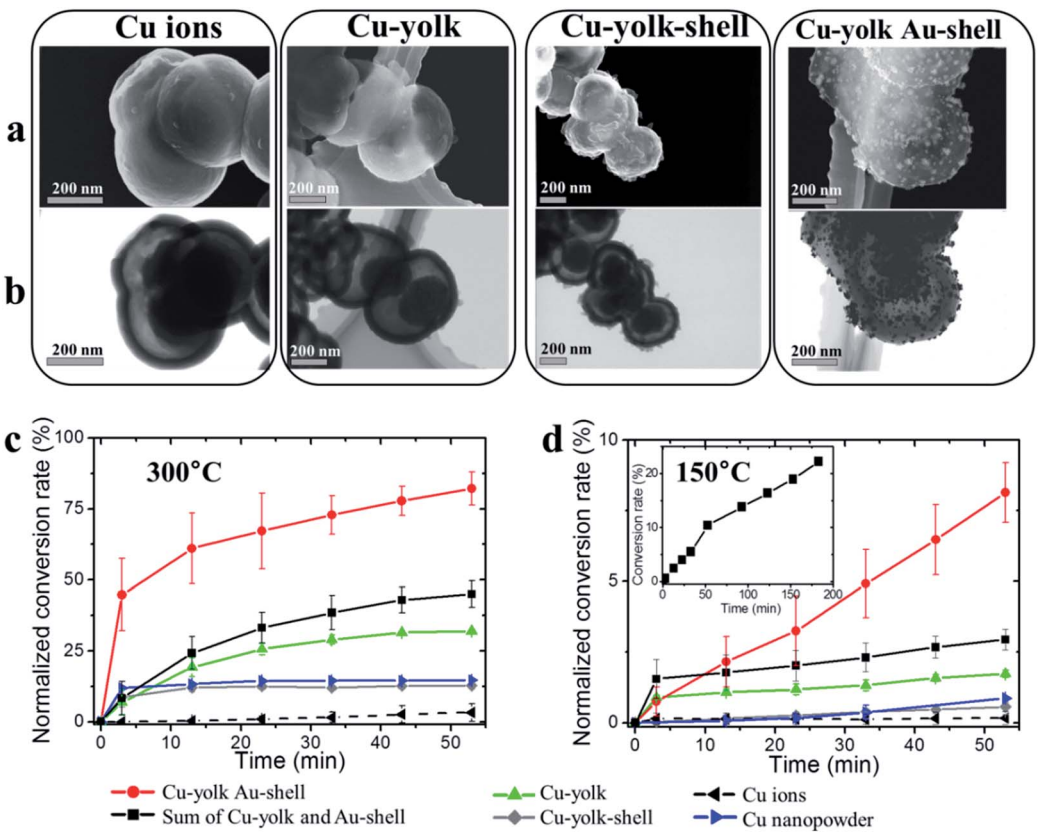

Fig. 6 Systematic investigation of catalytic activities. STEM micrographs, in scanning (a) and transmission (b) modes of different hierarchically loaded PANI yolk–shell nanocapsules. The resulting conversion rate of CO oxidation, normalized by the copper content, at 300 °C (c) and 150 °C (d) with copper nanopowder (blue line) or when nanocapsules were filled with copper ions (dashed black line), Cu-yolk–shell (grey line), Cu-yolk (green line), (Cu yolk Au shell) (red line) and the performance sum of Cu-yolk and Au-shell samples (black line). The inset in (d) shows the evolution of the normalized oxidation rate of CO with (Cu yolk Au shell) nanocapsules for 180 minutes.

Cu-yolk–shell nanocapsules exhibited a catalytic activity similar to commercial copper NPs, reaching around 10% oxidation rate at 300 °C and a negligible activity at 150 °C after 53 minutes. Normalized conversion rates reached a rapid saturation. Easily accessible copper NPs seemed thus to lead to limited catalysis performances. In this regard, the lack of structuring of the Cu-yolk–shell nanocapsule catalyst likely restricts any possible performance improvements over the commercial copper nanopowder. However, when Cu-yolk nanocapsules were used, the normalized oxidation rate was more than double compared with the non-structured controls at both considered temperatures, reaching around 30% at 300 °C (Fig. 7). This result suggests that a confinement effect operates, leading to both improved performances and a less rapid saturation of the activity rate. All polymer PANI yolk–shell nanocapsules appear thus as promising tools for improving the catalyst activity by controlling its nanostructure.

Significance of the hierarchical architecture. Co-loading the yolk–shell nanocapsules, in a hierarchical way, with both copper and gold metallic centers, was performed to probe any cooperative effect within the catalyst. To fairly investigate this effect, the (Cu-yolk Au-shell) nanocapsules (red line of Fig. 6) were compared with Cu-yolk, Au-shell, and (Cu-yolk Cu-shell) systems. At both considered temperatures, (Cu-yolk Au-shell) nanocapsules performed 7 times better than the non-structured (Cu-yolk Cu-shell) catalyst (Fig. 6c and d). A normalized conversion rate of 82% was achieved at 300 °C after 53 minutes and saturation of the performances seemed to be largely suppressed. At 150 °C, results were even more striking with a quasi-linear evolution of the normalized conversion rate with catalysis time, reaching more than 20% after 180 minutes while other catalysts levelled off at less than 2% (Fig. 6d in inset and S-17†). To be sure that these improved performances were not due to the sole presence of gold NPs on the shell, the activity of Au-shell nanocapsules was investigated, reaching a total (non-normalized) conversion rate of 13% at 300 °C and 1.7% at 150 °C after 53 minutes (Fig. S-18†). As a consequence, if the decoration of the shell part of the nanocapsules with Au NPs clearly modified their morphology and exposed their surface area for catalysis, it did not exhibit a significant catalytic activity by itself. By comparing the performance achieved by the (Cu-yolk Au-shell) catalyst with the sum of performances of the Au-shell and Cu-yolk samples, it is possible to empirically detect an eventual cooperative effect (Fig. 7). At both considered temperatures, the hierarchically loaded catalyst performed around two times better than the sum of its components (Fig. 7). These results are attributed to a cooperative effect between gold and copper particles in the hierarchically loaded (Cu-yolk Au-shell) nanocapsules that may reduce catalytic center inhibition by CO_2, as recently described by Epron *et al.*[56] In addition, a participation of PANI to this effect cannot be excluded as it is known to activate O_2,[51,52,57] trap CO[53,54] and even be a part of synergetic oxidation processes.[58] Following the same synthesis strategy, copper was replaced with nickel, leading to Ni-yolk and (Ni-yolk, Au-shell) nanocapsules to be compared with a Ni-yolk–shell, Au-shell and commercial nickel nanopowder (Fig. S-19 and S-20†). The normalized conversion rate for CO oxidation followed the same trend for both confinement effect and cooperative effect. These results confirm the functionalization versatility of nanostructured yolk–shell PANI. As an example, the shell layer functionalization was also tuned, by depositing platinum rather than gold (Fig. S-21).† This strategy of hierarchical loading, reduction and confinement of specific elements in nanostructured matrices could thus allow the specific adaptation of catalyst functions according to reaction needs.

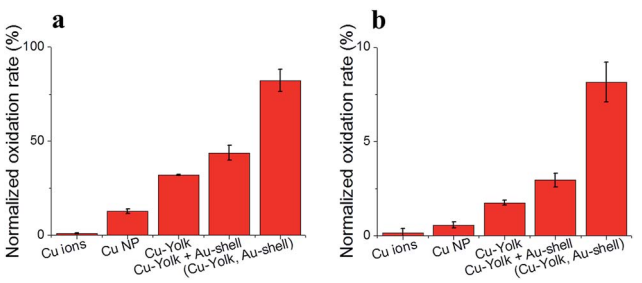

Fig. 7 Normalized oxidation rate reached after 53 min. Normalized CO oxidation rate reached after 53 min at 300 °C (a) and 150 °C (b) when the nanocapsules were loaded with copper ions, copper NPs, yolk-confined copper NPs (Cu-yolk), separately measured Cu-yolk and Au-shell, or hierarchically integrated (Cu-yolk Au-shell).

Conclusions

Self-assembled yolk–shell PANI nanocapsules were used for designing hierarchically loaded nanostructured catalysts containing copper, nickel and gold NP. Owing to the PANI matrix properties and the specific yolk–shell architecture, the yolk confinement of either copper or nickel NP was performed. As a result, catalysis performances were doubled compared with non-structured catalysts, owed to the introduction of confinement effects. When the hierarchical loading of yolk–shell nanocapsules was performed with different metals, both confinement and cooperative effects for CO oxidation were observed. Catalytic performances of nanocapsules loaded with (Cu-yolk, Au-shell) were around 7 times higher than the control. Even at low temperature (150 °C), a normalized oxidation rate of 20% could be achieved. The synthesis strategy is adaptable and (Cu-yolk Au-shell), (Ni-yolk Au-shell) and (Pt-shell) systems were studied here. The concept of hierarchical trapping, reduction and confinement of catalytic centers in active nanostructured matrices is thus believed to provide a versatile tool for designing adapted catalysts with confinement and cooperative effects.

Acknowledgements

We would like to thank Dr Satoshi Kawada, Dr Hirohito Ohata and the Material Analysis Station (NIMS) for ICP and XPS measurements. This work was supported by the International Center for Young Scientists (ICYS), the Japanese Society for the Promotion of Science (JSPS) and the World Premier International Research Center Initiative (WPI Initiative), MEXT, Japan. Dr Sanchez-Ballester and Dr Rydzek contributed equally to this work.

Notes and references

1 S. Royer and D. Duprez, *ChemCatChem*, 2011, **3**, 24–65.
2 G. Ferey, *Chem. Soc. Rev.*, 2008, **37**, 191–214.
3 Y.-G. Guo, J.-S. Hu and L.-J. Wan, *Adv. Mater.*, 2008, **20**, 2878–2887.
4 R. Bashyam and P. Zelenay, *Nature*, 2006, **443**, 63–66.
5 Y. Li and J. Shi, *Adv. Mater.*, 2014, **26**, 3176–3205.
6 P. R. Gil, L. L. del Mercato, P. del_Pino, A. Muñoz_Javier and W. J. Parak, *Nano Today*, 2008, **3**, 12–21.
7 C. Bai and M. Liu, *Nano Today*, 2012, **7**, 258–281.
8 C. Yu and J. He, *Chem. Commun.*, 2012, **48**, 4933–4940.
9 X. Pan and X. Bao, *Acc. Chem. Res.*, 2011, **44**, 553–562.
10 F. Goettmann and C. Sanchez, *J. Mater. Chem.*, 2007, **17**, 24–30.
11 Q. Zhang, I. Lee, J. B. Joo, F. Zaera and Y. Yin, *Acc. Chem. Res.*, 2013, **46**, 1816–1824.
12 S. Alayoglu, A. U. Nilekar, M. Mavrikakis and B. Eichhorn, *Nat. Mater.*, 2008, **7**, 333–338.
13 S. H. Joo, J. Y. Park, C.-K. Tsung, Y. Yamada, P. Yang and G. A. Somorjai, *Nat. Mater.*, 2009, **8**, 126–131.
14 F. Tao, M. E. Grass, Y. Zhang, D. R. Butcher, J. R. Renzas, Z. Liu, J. Y. Chung, B. S. Mun, M. Salmeron and G. A. Somorjai, *Science*, 2008, **322**, 932–934.
15 M. B. Gawande, R. Zboril, V. Malgras and Y. Yamauchi, *J. Mater. Chem. A*, 2015, **3**, 8241–8245.
16 V. Malgras, Q. Ji, Y. Kamachi, T. Mori, F.-K. Shieh, K. C.-W. Wu, K. Ariga and Y. Yamauchi, *Bull. Chem. Soc. Jpn.*, 2015, **88**, 1171–1200.
17 K. Lee, S. Cho, S. Heum Park, A. J. Heeger, C.-W. Lee and S.-H. Lee, *Nature*, 2006, **441**, 65–68.
18 G. Ciric-Marjanovic, *Synth. Met.*, 2013, **177**, 1–47.
19 X. Guo, G. T. Fei, H. Su and L. D. Zhang, *J. Mater. Chem.*, 2011, **21**, 8618–8625.
20 L. Huang, X. Yu, L. Gao, L. Chen, J. Wei and S. Xing, *New J. Chem.*, 2014, **38**, 3029.
21 H. Li, J. V. John, S. J. Byeon, M. S. Heo, J. H. Sung, K.-H. Kim and I. Kim, *Prog. Polym. Sci.*, 2014, **39**, 1878–1907.
22 G. Rydzek, T. G. Terentyeva, A. Pakdel, D. Golberg, J. P. Hill and K. Ariga, *ACS Nano*, 2014, **8**, 5240–5248.
23 Y. Guo, Y.-T. Xu, B. Zhao, T. Wang, K. Zhang, M. M. F. Yuen, X.-Z. Fu, R. Sun and C.-P. Wong, *J. Mater. Chem. A*, 2015, **3**, 13653–13661.
24 G. Lan, X. Zhang, X. Zhang, M. Li, Y. Li and Q. Yang, *RSC Adv.*, 2015, **5**, 35730–35736.
25 J. Han, M. Wang, R. Chen, N. Han and R. Guo, *Chem. Commun.*, 2014, **50**, 8295–8298.
26 G. Rydzek, Q. Ji, M. Li, P. Schaaf, J. P. Hill, F. Boulmedais and K. Ariga, *Nano Today*, 2015, **10**, 138–167.
27 V. Divya and M. V. Sangaranarayanan, *Eur. Polym. J.*, 2012, **48**, 560–568.
28 J. Stejskal, P. Kratochvíl and N. Radhakrishnan, *Synth. Met.*, 1993, **61**, 225–231.
29 J. Stejskal, *Chem. Pap.*, 2013, **67**, 814–848.
30 L. Gao, S. Lv and S. Xing, *Synth. Met.*, 2012, **162**, 948–952.
31 C. A. Amarnath, J. Kim, K. Kim, J. Choi and D. Sohn, *Polymer*, 2008, **49**, 432–437.
32 H. Sun, X. Shen, L. Yao, S. Xing, H. Wang, Y. Feng and H. Chen, *J. Am. Chem. Soc.*, 2012, **134**, 11243–11250.
33 G. Ciric-Marjanovic, *Synth. Met.*, 2013, **170**, 31–56.
34 O. P. Dimitriev, *Polym. Bull.*, 2003, **50**, 83–90.
35 J. E. Albuquerque, L. H. C. Mattoso, D. T. Balogh, R. M. Faria, J. G. Masters and A. G. MacDiarmid, *Synth. Met.*, 2000, **113**, 19–22.
36 C. Yang and C. Chen, *Synth. Met.*, 2005, **153**, 133–136.
37 G. Rydzek, L. Jierry, A. Parat, J. Thomann, J. Voegel, B. Senger, J. Hemmerlé, A. Ponche, B. Frisch, P. Schaaf and F. Boulmedais, *Angew. Chem., Int. Ed.*, 2011, **50**, 4374–4377.
38 F. Caruso, D. N. Furlong, K. Ariga, I. Ichinose and T. Kunitake, *Langmuir*, 1998, **14**, 4559–4565.
39 L. Xi, D. Ren, J. Luo and Y. Zhu, *J. Electroanal. Chem.*, 2010, **650**, 127–134.
40 M. U. A. Prathap, T. Pandiyan and R. Srivastava, *J. Polym. Res.*, 2013, **20**, 83.
41 J. Han, L. Li and R. Guo, *Macromolecules*, 2010, **43**, 10636–10644.
42 D. Briggs, *Handbook of X-ray Photoelectron Spectroscopy*, ed. C. D. Wanger, W. M. Riggs, L. E. Davis, J. F. Moulder and G. E. Muilenberg, Perkin-Elmer Corp., Physical Electronics Division, Eden Prairie, Minnesota, USA, 1979, vol. 3, pp. 190–195, 1981.
43 L. S. Dake, D. E. King and A. W. Czanderna, *Solid State Sci.*, 2000, **2**, 781–789.
44 P. Marcus and M. E. Bussell, *Appl. Surf. Sci.*, 1992, **59**, 7–21.
45 D. T. Thompson, *Nano Today*, 2007, **2**, 40–43.
46 G. G. Jernigan and G. A. Somorjai, *J. Catal.*, 1994, **147**, 567–577.
47 D. Hibbitts and E. Iglesia, *Acc. Chem. Res.*, 2015, **48**, 1254–1262.
48 J. Fonseca, S. Royer, N. Bion, L. Pirault-Roy, M. do C. Rangel, D. Duprez and F. Epron, *Appl. Catal., B*, 2012, **128**, 10–20.
49 H. C. Lee and D. H. Kim, *Catal. Today*, 2008, **132**, 109–116.
50 S. Scirè, C. Crisafulli, P. M. Riccobene, G. Patanè and A. Pistone, *Appl. Catal., A*, 2012, **417–418**, 66–75.
51 E. Vayner, H. Schweiger and A. B. Anderson, *J. Electroanal. Chem.*, 2007, **607**, 90–100.
52 J. Yano, K. Terayama and S. Yamasaki, *Synth. Met.*, 1997, **85**, 1381–1382.
53 J. da S. L. Fonseca, H. S. Ferreira, N. Bion, L. Pirault-Roy, M. do C. Rangel, D. Duprez and F. Epron, *Catal. Today*, 2012, **180**, 34–41.
54 N. Densakulprasert, L. Wannatong, D. Chotpattananont, P. Hiamtup, A. Sirivat and J. Schwank, *Mater. Sci. Eng., B*, 2005, **117**, 276–282.
55 C. Liu, Z. Noda, K. Sasaki and K. Hayashi, *Int. J. Hydrogen Energy*, 2012, **37**, 13529–13535.
56 J. da S. L. Fonseca, H. S. Ferreira, N. Bion, L. Pirault-Roy, M. do C. Rangel, D. Duprez and F. Epron, *Catal. Today*, 2012, **180**, 34–41.
57 V. Z. Barsukov, V. G. Khomenko, A. S. Katashinskii and T. I. Motronyuk, *Russ. J. Electrochem.*, 2004, **40**, 1170–1173.
58 X. Lu, X. Bian, Z. Li, D. Chao and C. Wang, *Sci. Rep.*, 2013, **3**, 2955.